Universität Stuttgart

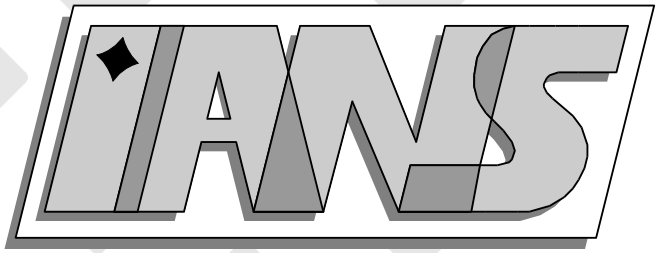

Second Order Lagrange Multiplier Spaces for Mortar Finite Elements in 3D

Bishnu P. Lamichhane, Barbara I. Wohlmuth

Berichte aus dem Institut für Angewandte Analysis und Numerische Simulation

Preprint 2003/007

Universität Stuttgart

Second Order Lagrange Multiplier Spaces for Mortar Finite Elements in 3D

Bishnu P. Lamichhane, Barbara I. Wohlmuth

Berichte aus dem Institut für Angewandte Analysis und Numerische Simulation

Preprint 2003/007

Institut für Angewandte Analysis und Numerische Simulation (IANS)
Fakultät Mathematik und Physik
Fachbereich Mathematik
Pfaffenwaldring 57
D-70 569 Stuttgart

E-Mail: ians-preprints@mathematik.uni-stuttgart.de
WWW: http://preprints.ians.uni-stuttgart.de

ISSN **1611-4176**

Second Order Lagrange Multiplier Spaces for Mortar Finite Elements in 3D

Bishnu P. Lamichhane* and Barbara I. Wohlmuth*

Abstract

Domain decomposition techniques provide a flexible tool for the numerical approximation of partial differential equations. Here, we consider mortar techniques for quadratic finite elements in 3D with different Lagrange multiplier spaces. In particular, we focus on Lagrange multiplier spaces which yield optimal discretization schemes and a locally supported basis for the associated constrained mortar spaces. As a result, standard efficient iterative solvers as multigrid methods can be easily adapted to the nonconforming situation. We present the discretization errors in different norms for linear and quadratic mortar finite elements with different Lagrange multiplier spaces. Numerical results illustrate the performance of our approach.

Key words. mortar finite elements, Lagrange multiplier, dual space, domain decomposition, nonmatching triangulation.
AMS subject classification. 65N30, 65N55.

1 Introduction

The coupling of different discretization schemes or of nonmatching triangulations can be analyzed within the framework of mortar methods. These nonconforming domain decomposition techniques provide a more flexible approach than standard conforming approaches. The nonconforming approach is of particular interest in many situations, for example, in problems with discontinuous diffusion coefficients and local anisotropies, when different parameters dominate different parts of the simulation domain or different discretization schemes are used in different subdomains. A complex global domain can be decomposed into several small subdomains of simple structure, and these subdomains can be meshed independently. To obtain a stable and optimal discretization scheme for the global problem, the information transfer among the subdomains has to be analyzed. Mortar methods were originally introduced to couple spectral and finite element approximations, see [BDM90, BMP93]. An optimal a priori estimate in the H^1-norm for the mortar finite element method has been established in [BMP93, BMP94, Ben99, BM97]. The analysis of three-dimensional mortar finite elements is given in [BM97, KLPV01, BD98], and a hp version is studied in [SS00]. In the linear 3D case, the stability of the mortar projection for the standard Lagrange multiplier space is established in [BD98], where also a multigrid

*This work was supported in part by the Deutsche Forschungsgemeinschaft, SFB 404, C12.

method for the saddle point problem is discussed. The main idea of the mortar technique is to replace the strong continuity condition of the solution across the interface by a weak one. Here, we consider mortar methods for second order finite elements in 3D. We focus on Lagrange multiplier spaces which yield locally supported basis functions of the constrained mortar space.

The paper is organized as follows: In the rest of this section, we present our model problem and briefly review the mortar method. In Section 2, we give some sufficient conditions on Lagrange multiplier spaces for quadratic finite elements and show the optimality of the approach. In Section 3, we present some examples of Lagrange multiplier spaces for quadratic finite elements for hexahedral triangulations. In contrast to earlier approaches, we use Lagrange multiplier spaces yielding a sparse inverse of the mass matrix. We also use the so-called dual Lagrange multiplier spaces which are biorthogonal to the trace of the finite element space at the interface. Unfortunately, a locally defined dual Lagrange multiplier space containing the bilinear hat functions does not exist for the serendipity elements. In that case, we augment the space by face bubble functions. Finally in Section 4, we present some numerical results in 3D for different Lagrange multiplier spaces illustrating the flexibility and performance of our approach. In particular, we consider the discretization errors in the L^2-norm, the energy norm and in a weighted L^2-norm for the Lagrange multiplier.

We consider the following elliptic second order boundary value problem

$$\begin{aligned} -\mathrm{div}(a\nabla u) + cu &= f, \quad \text{in } \Omega, \\ u &= 0, \quad \text{on } \partial\Omega, \end{aligned} \tag{1}$$

where $0 < a_0 \leq a \in L^\infty(\Omega)$, $f \in L^2(\Omega)$, $0 \leq c \in L^\infty(\Omega)$, and $\Omega \subset \mathbb{R}^3$ is a bounded polyhedral domain. The domain Ω is decomposed into K non-overlapping polyhedral subdomains Ω_k, $k = 1, \cdots, K$, such that

$$\overline{\Omega} = \bigcup_{k=1}^{K} \overline{\Omega}_k \quad \text{with} \quad \Omega_i \cap \Omega_j = \emptyset \quad \text{for} \quad i \neq j.$$

Here, we consider only geometrically conforming situations where the intersection between the boundaries of any two different subdomains $\partial\Omega_l \cap \partial\Omega_k$, $k \neq l$, is either empty, a common edge or a face. We define $\bar{\Gamma}_{kl} := \partial\Omega_k \cap \partial\Omega_l$, $1 \leq k, l \leq K$, the intersection of the boundaries of two subdomains and select only disjoint and non-empty interfaces γ_k, $1 \leq k \leq N$. Moreover, each γ_k can be associated with a couple $1 \leq k_1 < k_2 \leq K$ such that $\bar{\gamma}_k = \partial\Omega_{k_1} \cap \partial\Omega_{k_2}$. On each subdomain, we define

$$H^1_*(\Omega_k) := \{v \in H^1(\Omega_k), v_{|_{\partial\Omega \cap \partial\Omega_k}} = 0\}, \quad k = 1, \cdots, K$$

and consider the unconstrained product space

$$X := \prod_{k=1}^{K} H^1_*(\Omega_k).$$

To impose a weak matching condition on the interface, a Lagrange multiplier space $M := \prod_{k=1}^{N} H^{-1/2}(\gamma_k)$ is introduced on the skeleton

$$\Gamma = \bigcup_{k=1}^{N} \gamma_k.$$

Then, the weak matching condition on the skeleton Γ is realized in terms of the L^2-orthogonality of the jump $[u]$ of the solution across the interface and the Lagrange multiplier space M

$$\int_\Gamma [u]\,\mu\,d\sigma = 0, \quad \mu \in M.$$

Each subdomain Ω_k is associated with a shape regular family of hexahedral triangulations $\mathcal{T}_{k;h_k}$, the meshsize of which is bounded by h_k. We denote the discrete space of conforming piecewise triquadratic finite elements or of serendipity elements on Ω_k associated with $\mathcal{T}_{k;h_k}$ by $X_{h_k} \subset H^1_*(\Omega_k)$. Now, the unconstrained finite element space X_h can be written as

$$X_h := \prod_{k=1}^{K} X_{h_k}.$$

Each interface γ_k inherits a two-dimensional triangulation $\mathcal{S}_{k;h_k}$ either from $\mathcal{T}_{k_1;h_{k_1}}$ or $\mathcal{T}_{k_2;h_{k_2}}$. The subdomain from which the interface inherits its triangulation is called slave or non-mortar side, the opposite one master or mortar side. In the following, we denote the index of the slave side by $s(k)$ and the one of the master side by $m(k)$. Hence, the elements of $\mathcal{S}_{k;h_k}$ are boundary faces of $\mathcal{T}_{s(k);h_{s(k)}}$ with a meshsize bounded by $h_{s(k)}$. Furthermore, we assume that the mesh on Γ is globally quasi-uniform, and each element in $\mathcal{S}_{k;h_k}$, $k = 1, \cdots, N$, can be affinely mapped to the reference element $\hat{T} := (0,1) \times (0,1)$. The discrete Lagrange multiplier space M_h on Γ is defined as $M_h := \prod_{k=1}^{N} M_h(\gamma_k)$. Then, the discrete weak matching condition for $v_h \in X_h$ can be written as

$$\int_{\gamma_k} [v_h]\,\mu_i\,d\sigma = 0, \quad 1 \le i \le n_k,\ 1 \le k \le N, \tag{2}$$

where $n_k := \dim M_h(\gamma_k)$ and $\{\mu_i\}_{1\le i\le n_k}$ forms a basis of $M_h(\gamma_k)$. Here, $[v_h]$ is the jump of the function v_h on γ_k from the master side to the slave side. As usual, $\|\cdot\|_{s,\Omega_k}$ and $(\cdot,\cdot)_{s,\Omega_k}$ denote the norm and the corresponding inner product on $H^s(\Omega_k)$, respectively, and $|\cdot|_{s,\Omega_k}$ stands for the seminorm. The norm on $H^{1/2}_{00}(\gamma_k)$ and its dual space $H^{-1/2}(\gamma_k)$ will be denoted by $\|\cdot\|_{H^{1/2}_{00}(\gamma_k)}$ and $\|\cdot\|_{-1/2,\gamma_k}$, respectively. We define the broken norm $\|\cdot\|_s$ on X and the broken dual norm $\|\cdot\|_M$ on M by

$$\|u\|_s^2 := \sum_{k=1}^{K} \|u\|^2_{s,\Omega_k}, \quad \text{and} \quad \|\mu\|_M^2 := \sum_{k=1}^{N} \|\mu\|^2_{-1/2,\gamma_k},$$

respectively. There are two main approaches to obtain the mortar solution $u_h \in X_h$ of a discrete variational problem. The first one is based on the positive definite variational problem on the constrained finite element space which is given by means of the global Lagrange multiplier space M_h

$$V_h := \{v_h \in X_h \mid b(v_h, \mu_h) = 0,\ \mu_h \in M_h\},$$

where $b(v_h, \mu_h) := \sum_{k=1}^{N} \int_{\gamma_k} [v_h]\,\mu_h\,d\sigma$. We remark that the elements of the space V_h satisfy a weak continuity condition on the skeleton Γ in terms of discrete Lagrange multiplier space M_h. However, V_h is, in general, not a subspace of $H^1_0(\Omega)$. Then, the variational formulation of the mortar method can be given in terms of the constrained space V_h: find $u_h \in V_h$ such that

$$a(u_h, v_h) = (f, v_h)_0, \quad v_h \in V_h. \tag{3}$$

Here, the bilinear form $a(\cdot,\cdot)$ is defined as

$$a(v,w) := \sum_{k=1}^{K} \int_{\Omega_k} a\nabla v \cdot \nabla w + cv\, w\, dx.$$

The second approach is based on enforcing the weak continuity condition on the skeleton Γ as an additional variational equation which leads to a saddle point problem on the unconstrained product space X_h, see [Ben99]: find $(u_h, \lambda_h) \in X_h \times M_h$ such that

$$\begin{array}{lllll} a(u_h, v_h) + & b(v_h, \lambda_h) & = & (f, v_h)_0, & v_h \in X_h, \\ b(u_h, \mu_h) & & = & 0, & \mu_h \in M_h \ . \end{array} \tag{4}$$

It is clear that the choice of the discrete Lagrange multiplier space M_h plays an essential role for the stability of the saddle point problem and the optimality of the discretization scheme. The Lagrange multiplier space has to be large enough to obtain an optimal consistency error, and it has to be small enough to get an optimal best approximation error and a suitable discrete inf-sup condition. In the next section, we state sufficient conditions on the Lagrange multiplier space for quadratic finite elements to get optimal a priori estimates. Here, the nodal Lagrange multiplier basis functions are defined locally and are associated with the interior nodes of the mesh on $\gamma_k, k = 1, \cdots, N$. Now, we group the degrees of freedom of X_h associated with the skeleton Γ into two groups $u_{h|\Gamma} := (u_m, u_s)$, where u_m contains all nodal values of u_h on the master sides and all nodal values at the nodes on the boundary of the interface γ_k on the slave sides, and u_s consists of all nodal values of u_h at the interior nodes of γ_k on the slave sides, $1 \le k \le N$, see Figure 1. The associated sets of nodes are called $\mathcal{N}_m$ and $\mathcal{N}_s$, respectively. Furthermore, we denote by $\mathcal{N}_h$ the set of all nodes in X_h and we set $\mathcal{N}_i := \mathcal{N}_h \backslash (\mathcal{N}_m \cup \mathcal{N}_s)$. The corresponding nodal values of u_h in $\mathcal{N}_i$ will be denoted by a block vector u_i. Then (2) can be written in its algebraic form as

$$M_s u_s + M_m u_m = 0. \tag{5}$$

The entries of the mass matrices are given by $m_{ij} := \int_{\gamma_k} [\phi_j]\, \mu_i\, d\sigma$, where ϕ_j are the finite

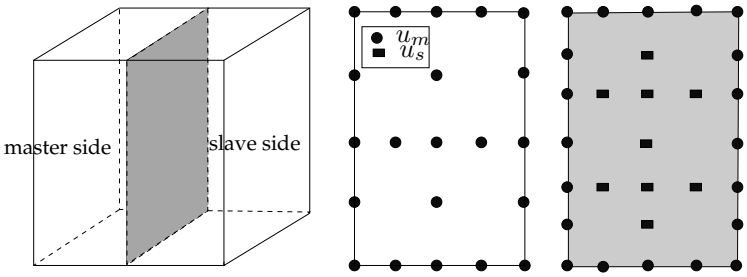

Figure 1: Decomposition into u_m and u_s for the serendipity elements

element basis functions corresponding to the different groups of nodes, and μ_i denote the basis functions of M_h. Since the basis functions have a local support, the mass matrices are sparse. Formally, we can obtain the values on the slave side as $u_s = -M_s^{-1} M_m u_m$. Although M_s is a sparse matrix, the inversion of M_s is, in general, expensive, and M_s^{-1} is

dense. This observation motivates our interest in Lagrange multiplier spaces which yield a sparse inverse of the mass matrix M_s. A natural choice is a dual Lagrange multiplier space, see, e.g., [Woh01], having a diagonal mass matrix M_s. Then, the basis functions $\{\mu_i\}_{1\leq i\leq n_k}$ of $M_h(\gamma_k)$ and $\{\varphi_i\}_{1\leq i\leq n_k}$ of the trace space $W_{0,h}(\gamma_k)$ having the zero boundary condition on $\partial\gamma_k$ satisfy the biorthogonality relation

$$\int_{\gamma_k} \mu_i \, \varphi_j \, d\sigma = \delta_{ij} \int_{\gamma_k} \varphi_j \, d\sigma, \quad 1 \leq i, j \leq n_k. \tag{6}$$

If M_s is a sparse triangular matrix, the inverse of M_s is also a sparse triangular matrix. Hence, to get a sparse inverse of mass matrix M_s, it is enough to work with a Lagrange multiplier space which yields a sparse triangular mass matrix M_s. We define the product space $W_{0,h}$ as

$$W_{0,h} := \prod_{k=1}^{N} W_{0,h}(\gamma_k),$$

and the broken $H_{00}^{1/2}$-norm on $W_{0,h}$ is denoted by

$$\|v\|_W^2 := \sum_{k=1}^{N} \|v\|_{H_{00}^{1/2}(\gamma_k)}^2.$$

2 A priori estimates

In this section, we give some assumptions on quadratic Lagrange multiplier spaces which guarantee optimal a priori estimates. Following a similar approach as in [KLPV01], we impose the following assumptions on the discrete Lagrange multiplier spaces for quadratic finite elements

[P0] $\dim W_{0,h}(\gamma_k) = \dim M_h(\gamma_k), \quad 1 \leq k \leq N.$

[P1] There is a constant C independent of the triangulation such that

$$\inf_{\mu\in M_h(\gamma_k)} \|v-\mu\|_{0,\gamma_k} \leq C h_{s(k)}^2 |v|_{2,\gamma_k}, \quad v \in H^2(\gamma_k), \quad 1 \leq k \leq N.$$

[P2] There is a constant C independent of the triangulation such that

$$\|\theta\|_{0,\gamma_k} \leq C \sup_{\mu\in M_h(\gamma_k)\setminus\{0\}} \frac{(\theta,\mu)_{0,\gamma_k}}{\|\mu\|_{0,\gamma_k}}, \quad \theta \in W_{0,h}(\gamma_k), \quad 1 \leq k \leq N.$$

It follows from assumption [P1] that $\mathcal{P}_1(\gamma_k) \subset M_h(\gamma_k)$ for all $k = 1, \cdots, N$, where $\mathcal{P}_1(\gamma_k)$ is the space of linear functions on γ_k. For each γ_k, the mortar projection $\Pi_k : L^2(\gamma_k) \to W_{0,h}(\gamma_k)$ is defined as

$$\int_{\gamma_k} \Pi_k v \, \mu \, d\sigma = \int_{\gamma_k} v \, \mu \, d\sigma, \quad \mu \in M_h(\gamma_k). \tag{7}$$

The stability of the mortar projection is essential for the optimality of the best approximation error.

Lemma 1. *Under the assumptions [P0] and [P2], the mortar projection* (7) *is stable in the L^2-norm. Furthermore, if $w \in H_0^1(\gamma_k)$*

$$\|\Pi_k w\|_{1,\gamma_k} \leq C\|w\|_{1,\gamma_k}.$$

Proof: By assumption [P2], we find that if $v \in W_{0,h}(\gamma_k)$ satisfies $(v,\mu)_{0,\gamma_k} = 0$ for all $\mu \in M_h(\gamma_k)$, then $v = 0$. Hence, the mortar projection is well-defined by the assumptions [P0] and [P2]. The L^2-stability of Π_k follows from

$$\|\Pi_k w\|_{0,\gamma_k} \leq C \sup_{\mu\in M_h(\gamma_k)\setminus\{0\}} \frac{(\Pi_k w,\mu)_{0,\gamma_k}}{\|\mu\|_{0,\gamma_k}} = C \sup_{\mu\in M_h(\gamma_k)\setminus\{0\}} \frac{(w,\mu)_{0,\gamma_k}}{\|\mu\|_{0,\gamma_k}} \leq C\|w\|_{0,\gamma_k}.$$

Now, using the L^2-stability and an inverse estimate, we find for $w \in H_0^1(\gamma_k)$

$$\begin{aligned}\|\Pi_k w\|_{1,\gamma_k} \leq \|\Pi_k w - Pw\|_{1,\gamma_k} + \|Pw\|_{1,\gamma_k} &\leq C\left(\frac{1}{h_{s(k)}}\|\Pi_k(w-Pw)\|_{0,\gamma_k} + \|w\|_{1,\gamma_k}\right)\\ &\leq C\left(\frac{1}{h_{s(k)}}\|w-Pw\|_{0,\gamma_k} + \|w\|_{1,\gamma_k}\right) \leq C\|w\|_{1,\gamma_k},\end{aligned}$$

where P denotes the L^2-projection onto $W_{0,h}(\gamma_k)$. ■

Using Lemma 1 and an interpolation argument, we obtain for $w \in H_{00}^{1/2}(\gamma_k)$,

$$\|\Pi_k w\|_{H_{00}^{1/2}(\gamma_k)} \leq C\|w\|_{H_{00}^{1/2}(\gamma_k)}.$$

In a next step, we provide the best approximation property of the space V_h. We use the ideas and techniques introduced in [BM97, BMP93].

Lemma 2. *Assume that the assumptions [P0]–[P2] hold. If $u \in H_0^1(\Omega)$ and $u_{|\Omega_k} \in H^3(\Omega_k)$ for all $k = 1,\cdots,K$, then there exists a constant C depending only on the ratio of the meshsizes of the master and slave sides such that*

$$\inf_{u_h\in V_h} \|u-u_h\|_1^2 \leq C\sum_{k=1}^{K} h_k^4\|u\|_{3,\Omega_k}^2.$$

Proof: Since $W_{0,h}(\gamma_k) \subset H_{00}^{1/2}(\gamma_k)$, each $v \in W_{0,h}(\gamma_k)$ can trivially be extended to a function $\tilde{v} \in H^{1/2}(\partial\Omega_{s(k)})$. Let $\mathcal{H}_h\tilde{v} \in H^1(\Omega_{s(k)})$ be the discrete harmonic extension of $\tilde{v}$ on $\Omega_{s(k)}$. Then, $\|\mathcal{H}_h\tilde{v}\|_{1,\Omega_{s(k)}} \leq C\|\tilde{v}\|_{H^{1/2}(\partial\Omega_{s(k)})} \leq C\|v\|_{H_{00}^{1/2}(\gamma_k)}$. By means of this discrete harmonic extension, we define a discrete extension operator $E_k : W_{0,h}(\gamma_k) \to X_h$ for each γ_k as $E_k v := \mathcal{H}_h\tilde{v}$ on $\Omega_{s(k)}$, and $E_k v := 0$ elsewhere. Then

$$\|E_k v\|_1 \leq C\|v\|_{H_{00}^{1/2}(\gamma_k)}, \quad v \in W_{0,h}(\gamma_k). \tag{8}$$

Let $l_h u \in X_h$ be the Lagrange interpolant of u in X_h. It is easy to see that $v := l_h u + \sum_{k=1}^{N} E_k\Pi_k[l_h u]$ is an element of V_h. Then, we find

$$\|u-v\|_1 \leq \|u-l_h u\|_1 + \|\sum_{k=1}^{N} E_k\Pi_k[l_h u]\|_1.$$

By using (8) and a coloring argument, we have

$$\|\sum_{k=1}^{N} E_k \Pi_k [l_h u]\|_1^2 = \sum_{l=1}^{K} \|\sum_{k=1}^{N} E_k \Pi_k [l_h u]\|_{1,\Omega_l}^2 \leq C \sum_{k=1}^{N} \|\Pi_k [l_h u]\|_{H_{00}^{1/2}(\gamma_k)}^2.$$

We note that the constant C does not depend on the number of subdomains. Applying the $L^2(\gamma_k)$-stability of Π_k and an inverse estimate, we get

$$\begin{aligned} \|\Pi_k [l_h u]\|_{H_{00}^{1/2}(\gamma_k)}^2 \leq \frac{C}{h_{s(k)}} \|[l_h u]\|_{0,\gamma_k}^2 &\leq \frac{C}{h_{s(k)}} \left(\|(u - l_h u)_{|\Omega_{m(k)}}\|_{0,\gamma_k}^2 + \|(u - l_h u)_{|\Omega_{s(k)}}\|_{0,\gamma_k}^2 \right) \\ &\leq \frac{C}{h_{s(k)}} \left(h_{m(k)}^5 \|u\|_{3,\Omega_{m(k)}}^2 + h_{s(k)}^5 \|u\|_{3,\Omega_{s(k)}}^2 \right). \end{aligned}$$

Summing over all $k = 1, \cdots, N$, we obtain

$$\|\sum_{k=1}^{N} E_k \Pi_k [l_h u]\|_1^2 \leq C \left(h_{mr} \sum_{k=1}^{N} h_{m(k)}^4 \|u\|_{3,\Omega_{m(k)}}^2 + \sum_{k=1}^{N} h_{s(k)}^4 \|u\|_{3,\Omega_{s(k)}}^2 \right),$$

where

$$h_{mr} := \max \left\{ \frac{h_{m(k)}}{h_{s(k)}}, \quad 1 \leq k \leq N \right\}.$$

Finally, the lemma follows by using the interpolation property of $l_h u$. ■

We remark that in contrast to a convergence theory of mortar finite elements in 2D, the constant in the right hand side depends on the ratio of the meshsizes of master and slave sides. However, if the mesh on the wirebasket is conforming and u is continuous, we find $[l_h u] \in H_{00}^{1/2}(\gamma_k)$ and thus the $H_{00}^{1/2}$-stability of Π_k can be directly applied. In that case, the ratio does not enter in the upper bound, see [KLPV01]. Working with mesh dependent norms and a trivial extension shows that the global ratio h_{mr} can be replaced by a local one.

Theorem 3. *Let u and u_h be the solutions of the problems* (1) *and* (3)*, respectively. Assume that $u \in H_0^1(\Omega)$, $u_{|\Omega_k} \in H^3(\Omega_k)$ for $k = 1, \cdots, K$, and $[a \frac{\partial u}{\partial n}] = 0$ on Γ. Under the assumptions [P0]–[P2], there exists a constant C depending only on the ratio of the meshsizes of the master and the slave sides such that*

$$\|u - u_h\|_1^2 \leq C \sum_{k=1}^{K} h_k^4 \|u\|_{3,\Omega_k}^2.$$

Proof: The bilinear form $a(\cdot, \cdot)$ is continuous on X, and it is coercive on

$$B := \left\{ v \,|\, v \in H_*^1(\Omega_k), 1 \leq k \leq K, \text{ and } \int_{\gamma_k} [v] \, d\sigma = 0, \, 1 \leq k \leq N \right\},$$

see [BMP93]. Hence, assumption [P1] assures that $V_h \subset B$. Thus, Strang's Lemma [BS94] can be applied, and we get

$$\|u - u_h\|_1 \leq C \left(\inf_{v_h \in V_h} \|u - v_h\|_1 + \sup_{v_h \in V_h \setminus \{0\}} \frac{|a(u - u_h, v_h)|}{\|v_h\|_1} \right). \tag{9}$$

The first term in the right side of (9) denotes the best approximation error and the second one stands for the consistency error. Lemma 2 guarantees the required order for the best approximation error. Thus it is sufficient to consider the consistency error in more detail. Now, $a(u-u_h, v_h)$ can be written as

$$a(u-u_h, v_h) = \int_\Gamma a\frac{\partial u}{\partial n}\,[v_h]\,d\sigma = \sum_{k=1}^{N}\left(a\frac{\partial u}{\partial n_k}, [v_h]\right)_{0,\gamma_k}, \quad v_h \in V_h.$$

Here, $\frac{\partial u}{\partial n}$ is the outward normal derivative of u on Γ from the master side, and $\frac{\partial u}{\partial n} = \frac{\partial u}{\partial n_k}$ on γ_k. We take $\mu \in M_h(\gamma_k)$, then the definition of V_h yields

$$\left(a\frac{\partial u}{\partial n_k}, [v_h]\right)_{0,\gamma_k} = \left(a\frac{\partial u}{\partial n_k} - \mu, [v_h]\right)_{0,\gamma_k}.$$

Since $\mu \in M_h(\gamma_k)$ is arbitrary, we can bound the consistency error by

$$\left(a\frac{\partial u}{\partial n_k}, [v_h]\right)_{0,\gamma_k} \le \inf_{\mu\in M_h(\gamma_k)} \|a\frac{\partial u}{\partial n_k} - \mu\|_{\left(H^{1/2}(\gamma_k)\right)'} \|[v_h]\|_{1/2,\gamma_k}.$$

Let $Q : L^2(\gamma_k) \to M_h(\gamma_k)$ be the L^2-projection onto $M_h(\gamma_k)$. Using assumption [P2] and an interpolation between $L^2(\gamma_k)$ and $H^2(\gamma_k)$, we obtain

$$\|w - Qw\|_{0,\gamma_k} \le Ch_{s(k)}^{3/2}\|w\|_{3/2,\gamma_k}, \quad w \in H^{3/2}(\gamma_k).$$

In terms of a standard Aubin–Nitsche trick and the previous estimate, we get

$$\|w - Qw\|_{\left(H^{1/2}(\gamma_k)\right)'} \le Ch_{s(k)}^{1/2}\|w - Qw\|_{0,\gamma_k} \le Ch_{s(k)}^{2}\|w\|_{3/2,\gamma_k}.$$

Finally, the trace theorem yields

$$\begin{aligned}\left(a\frac{\partial u}{\partial n_k}, [v_h]\right)_{0,\gamma_k} &\le Ch_{s(k)}^2 \left\|\frac{\partial u}{\partial n_k}\right\|_{3/2,\gamma_k} \|[v_h]\|_{1/2,\gamma_k} \\ &\le Ch_{s(k)}^2\|u\|_{3,\Omega_{s(k)}}\left(\|v_h\|_{1,\Omega_{m(k)}} + \|v_h\|_{1,\Omega_{s(k)}}\right).\end{aligned}$$

Now, using the Cauchy–Schwarz inequality and summing over all $k = 1, \cdots, N$, we obtain

$$|a(u-u_h, v_h)| \le C\|v_h\|_1 \left(\sum_{k=1}^{K} h_k^4\|u\|_{3,\Omega_k}^2\right)^{1/2}.$$

■

To obtain an a priori estimate for the Lagrange multipliers, we follow exactly the same procedures as in [Ben99].

Lemma 4. *Assume that the Lagrange multiplier space M_h satisfies assumptions [P0]–[P2]. Then, for every $\mu \in M_h$, there exists a $v_\mu \in X_h$ such that*

$$\|v_\mu\|_1 \le C\|\mu\|_M, \quad \|\mu\|_M^2 \le Cb(v_\mu, \mu) \quad \textit{and} \quad \|[v_\mu]\|_W \le C\|\mu\|_M.$$

Proof: By means of the stability of the mortar projection, we get for $\mu \in M_h(\gamma_k)$

$$\begin{aligned}\|\mu\|_{-1/2,\gamma_k} &= \sup_{\varphi \in H_{00}^{1/2}(\gamma_k)\setminus\{0\}} \frac{(\mu,\varphi)_{0,\gamma_k}}{\|\varphi\|_{H_{00}^{1/2}(\gamma_k)}} \leq C \sup_{\varphi \in H_{00}^{1/2}(\gamma_k)\setminus\{0\}} \frac{(\mu,\Pi_k\varphi)_{0,\gamma_k}}{\|\Pi_k\varphi\|_{H_{00}^{1/2}(\gamma_k)}} \\ &= C \sup_{\varphi \in W_{0,h}(\gamma_k)\setminus\{0\}} \frac{(\mu,\varphi)_{0,\gamma_k}}{\|\varphi\|_{H_{00}^{1/2}(\gamma_k)}} \leq C(\mu,\tilde{\varphi}_k)_{0,\gamma_k} \end{aligned} \tag{10}$$

for some $\tilde{\varphi}_k \in W_{0,h}(\gamma_k)$ with $\|\tilde{\varphi}_k\|_{H_{00}^{1/2}(\gamma_k)} = 1$. Now, we extend $\tilde{\varphi}_k \in W_{0,h}(\gamma_k)$ to X_h by using the extension operator E_k as defined in Lemma 2 to get $E_k\tilde{\varphi}_k =: v_k \in X_h$. Then, we have

$$\|v_k\|_1 \leq C\|\tilde{\varphi}_k\|_{H_{00}^{1/2}(\gamma_k)} \quad \text{and} \quad 0 \leq (\mu,\tilde{\varphi}_k)_{0,\gamma_k} = b(v_k,\mu).$$

Setting $v_\mu := \sum_{k=1}^N b(v_k,\mu)v_k$ and using the fact that $\|v_k\|_1 \leq C$, we get

$$\begin{aligned}\|v_\mu\|_1^2 &= \|\sum_{k=1}^N b(v_k,\mu)v_k\|_1^2 = \sum_{l=1}^K \|\sum_{k=1}^N b(v_k,\mu)v_k\|_{1,\Omega_l}^2 \\ &\leq C\sum_{k=1}^N b(v_k,\mu)^2 \leq C\sum_{k=1}^N \|\mu\|_{-1/2,\gamma_k}^2 = C\|\mu\|_M^2.\end{aligned}$$

This proves the first assertion. Using a coloring argument, the constant C does not depend on the number of subdomains. Furthermore, summing the equation (10) over all interfaces γ_k, $k = 1,\cdots,N$, we obtain the second assertion

$$\|\mu\|_M^2 \leq C\sum_{k=1}^N b(v_k,\mu)^2 = Cb(v_\mu,\mu).$$

Finally, the third assertion follows from

$$\|[v_\mu]\|_W^2 = \sum_{k=1}^N b(v_k,\mu)^2\|[v_k]\|_{H_{00}^{1/2}(\gamma_k)}^2 = \sum_{k=1}^N b(v_k,\mu)^2 \leq \sum_{k=1}^N \|\mu\|_{-1/2,\gamma_k}^2\|[v_k]\|_{H_{00}^{1/2}(\gamma_k)}^2 = \|\mu\|_M^2.$$

■

The best approximation property, Lemma 4, assumption [P2] and the first equation of the saddle point problem give an a priori estimate for the Lagrange multipliers.

Lemma 5. *Under the assumptions of Theorem 3, we have*

$$\|\lambda - \lambda_h\|_M^2 \leq C\sum_{k=1}^K h_k^4\|u\|_{3,\Omega_k}^2.$$

3 Quadratic Lagrange multiplier spaces in 3D

In this section, we consider different possibilities for Lagrange multiplier spaces in 3D for quadratic finite elements with $\text{supp}\varphi_i = \text{supp}\mu_i$. In particular, we focus on the standard finite elements and the serendipity elements and restrict ourselves to hexahedral triangulations. These two finite elements have different degrees of freedom on the interface and therefore, the Lagrange multiplier spaces should be considered separately.

3.1 A dual Lagrange multiplier space for the standard triquadratic finite elements

In the case of a hexahedral triangulation, a dual Lagrange multiplier space in 3D for trilinear and triquadratic finite elements can be formed by taking the tensor product of the dual Lagrange multiplier space in 2D. Let $\hat{\varphi}_0$, $\hat{\varphi}_1$ and $\hat{\varphi}_2$ be the nodal quadratic finite element basis functions on the reference element $(0,1)$ in one dimension, where $\hat{\varphi}_0$ and $\hat{\varphi}_1$ are the basis functions corresponding to the left and the right vertices of the reference element, and $\hat{\varphi}_2$ is the basis function corresponding to the midpoint of the reference element. Then, the quadratic dual Lagrange multiplier basis functions on the reference element are defined by

$$\hat{\lambda}_0(t) := \hat{\varphi}_0(t) - \frac{3}{4}\hat{\varphi}_2(t) + \frac{1}{2}, \quad \hat{\lambda}_1(t) := \hat{\varphi}_1(t) - \frac{3}{4}\hat{\varphi}_2(t) + \frac{1}{2} \quad \text{and} \quad \hat{\lambda}_2(t) := \frac{5}{2}\hat{\varphi}_2(t) - 1.$$

The Lagrange multiplier basis functions for the element touching a crosspoint should be modified. In particular, if $t = 0$ is a crosspoint, we have

$$\hat{\lambda}_2(t) := -2t + 2, \quad \hat{\lambda}_1(t) := 2t - 1,$$

and if $t = 1$ is a crosspoint, we set

$$\hat{\lambda}_2(t) := 2t, \quad \hat{\lambda}_0(t) := 1 - 2t.$$

Furthermore, for a hat function ϕ_p^l at an interior vertex p, we find

$$\phi_p^l(t) = \mu_p(t) + \frac{1}{2}(\mu_{e1}(t) + \mu_{e2}(t)), \tag{11}$$

where μ_p is a Lagrange multiplier corresponding to the vertex p and μ_{e1} and μ_{e2} are the basis functions associated with the midpoints of the two adjacent edges. If p is a crosspoint, we have $\phi_p^l(t) = \frac{1}{2}\mu_e(t)$, where μ_e is the Lagrange multiplier basis function corresponding to the midpoint of the edge containing the crosspoint. Then, the Lagrange multiplier basis functions on the reference element $\hat{T} = (0,1) \times (0,1)$ having a tensor product structure are defined as

$$\hat{\lambda}_{ij}(x,y) := \hat{\lambda}_i(x)\hat{\lambda}_j(y).$$

Here, $\hat{\lambda}_{00}(x,y),\ \hat{\lambda}_{10}(x,y),\ \hat{\lambda}_{11}(x,y)$ and $\hat{\lambda}_{01}(x,y)$ are the Lagrange multipliers corresponding to the four vertices $(0,0), (1,0), (1,1)$ and $(0,1)$, and $\hat{\lambda}_{20}(x,y),\ \hat{\lambda}_{12}(x,y),\ \hat{\lambda}_{21}(x,y)$ and $\hat{\lambda}_{02}(x,y)$ are the ones corresponding to the midpoints $(0.5,0), (1,0.5), (0.5,1)$ and $(0,0.5)$ of the four edges, respectively, and finally $\hat{\lambda}_{22}(x,y)$ is the one corresponding to the center of gravity $(0.5,0.5)$ of the reference element. The Lagrange multiplier basis functions are associated with the vertices, midpoints of the edges and the center of gravity of elements in $\mathcal{S}_{k;h_k}, 1 \leq k \leq N$. The global basis functions μ_i are obtained by using an affine mapping and gluing the local ones together. All nodes on the boundary $\partial\gamma_k$ of γ_k are crosspoints and do not carry a degree of freedom for the Lagrange multiplier space. We note that we have to use the modification at the crosspoints to compute the tensor product for the Lagrange multipliers corresponding to the elements touching $\partial\gamma_k$. Observing (11), we find that the bilinear hat function at each vertex is contained in the Lagrange multiplier space $M_h(\gamma_k)$. We point out that this is also valid on $\partial\gamma_k$, although there are no degrees of freedom. Hence, assumption [P1] is satisfied. Assumption [P0] is trivially satisfied by construction. Now,

we verify assumption [P2]. Let $\varphi := \sum_{k=1}^{n_k} a_k \varphi_k$ be in $W_{0,h_k}(\gamma_k)$ and set $\mu := \sum_{k=1}^{n_k} a_k \mu_k$. In the following, we assume that $\hat{\varphi}_i$ and $\hat{\mu}_i$ are obtained from φ_i and μ_i by an affine mapping from the element T to the reference element $\hat{T}$. Now, by using the biorthogonality relation (6) and the quasi-uniformity assumption, we get

$$(\varphi, \mu)_{0,\gamma_k} = \sum_{i,j=1}^{n_k} a_i a_j (\varphi_i, \mu_j)_{0,\gamma_k} = \sum_{i=1}^{n_k} a_i^2 \int_{\gamma_k} \varphi_i \, d\sigma \geq C \sum_{i=1}^{n_k} a_i^2 h_{s(k)}^2 \geq C \|\varphi\|_{0,\gamma_k}^2.$$

Taking into account the fact that $\|\varphi\|_{0,\gamma_k}^2 \equiv \|\mu\|_{0,\gamma_k}^2 \equiv \sum_{i=1}^{n_k} a_i^2 h_{s(k)}^2$, we find that assumption [P2] is satisfied. Figure 2 shows the three different types of Lagrange multipliers on the reference element.

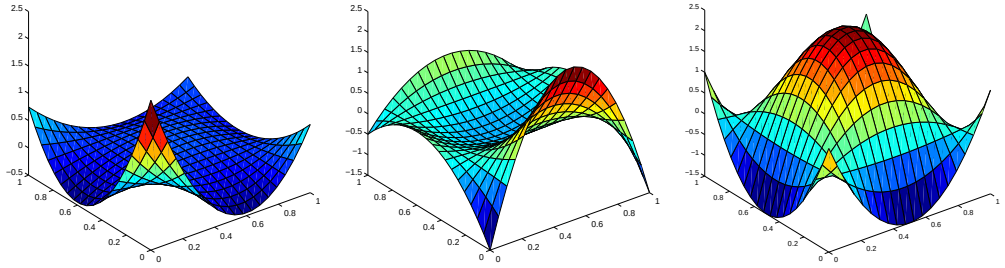

Figure 2: The Lagrange multipliers corresponding to a vertex (left), to an edge (middle) and to the center of gravity (left)

3.2 Serendipity elements and a dual Lagrange multiplier space

Here, we give a non-existence result for a dual Lagrange multiplier space for the serendipity elements. A similar result for simplicial triangulations and quadratic finite elements is given in [LW02]. We denote by $W_h^1(\gamma_k)$ the finite element space of piecewise bilinear hat functions on γ_k. In case of standard triquadratic finite elements, the dual Lagrange multiplier space with tensor product structure contains $W_h^1(\gamma_k)$. Unfortunately, there exists no dual Lagrange multiplier space for the serendipity elements yielding optimal a priori estimates with $\text{supp}\varphi_i = \text{supp}\mu_i$, where φ_i are the serendipity nodal finite element basis functions on the interface γ_k.

Lemma 6. *Under the assumption that $\text{supp}\varphi_i = \text{supp}\mu_i$, there exists no dual Lagrange multiplier space $M_h(\gamma_k)$ such that $W_h^1(\gamma_k) \subset M_h(\gamma_k)$.*

Proof: We prove this by contradiction. Assume that

$$\sum_i \alpha_i \mu_i = \phi_p^l, \tag{12}$$

where ϕ_p^l is the bilinear hat function associated with the interior vertex p having the coordinates $(0,0)$, see Figure 3. Suppose the coordinates of the four corners of the element T_1 be $(-1,0),(0,0),(0,1)$ and $(-1,1)$, and of the element T_2 be $(0,0),(1,0),(1,1)$ and $(0,1)$.

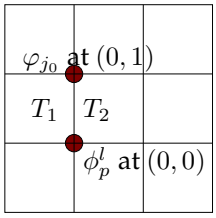

Figure 3: 2D interface of 3D hexahedral triangulation

Because of the duality, the functions μ_i are biorthogonal to the finite element basis functions φ_i on the interface. Hence, after multiplying (12) by some finite element basis function φ_j and integrating over the interface γ_k, we get

$$\alpha_j = \frac{\int_{\gamma_k} \varphi_j \phi_p^l \, d\sigma}{\int_{\gamma_k} \varphi_j \, d\sigma}.$$

Let j_0 be the interior vertex with coordinates $(0,1)$ such that j_0 and p share one edge, see Figure 3. Then, we can write

$$\int_{\gamma_k} \varphi_{j_0} \phi_p^l \, d\sigma = \int_{T_1} \varphi_{j_0} \phi_p^l \, d\sigma + \int_{T_2} \varphi_{j_0} \phi_p^l \, d\sigma = -\frac{1}{18}$$

and thus $\alpha_{j_0} \neq 0$. Since the basis functions μ_i are locally linearly independent, we obtain $\mathrm{supp}\mu_{j_0} \subseteq \mathrm{supp} \sum_i \alpha_i \mu_i$. By construction, we find $\mathrm{supp}\mu_{j_0} \subsetneq \mathrm{supp}\phi_p^l$, which contradicts (12). ■

3.3 Lagrange multiplier spaces for the serendipity elements

The previous subsection shows that there does not exist a dual Lagrange multiplier space for the serendipity elements containing the bilinear hat function at each vertex and satisfying $\mathrm{supp}\varphi_i = \mathrm{supp}\mu_i$. Here, we consider two different Lagrange multiplier spaces for the serendipity elements. The essential point is that the Lagrange multiplier space should lead to an optimal and stable discretization scheme. For this purpose, the assumptions [P0]–[P2] are crucial. The first idea is to choose a standard Lagrange multiplier space, see [BMP93, BMP94]. In this case, the basis functions for each interior element $T \in S_{k;h_k}$ of the interface γ_k (i.e., $T \in S_{k;h_k}$ with $\partial T \cap \partial\gamma_k = \emptyset$) are the serendipity elements in 2D. All nodes on $\partial\gamma_k$ do not carry a degree of freedom for the Lagrange multipliers. Therefore, in order to satisfy assumption [P1], it is necessary to modify the definition of the basis functions for the elements touching the boundary $\partial\gamma_k$ of the interface γ_k. Suppose an element $T \in S_{k;h_k}$ with $\partial T \cap \partial\gamma_k \neq \emptyset$ has n degrees of freedom for the Lagrange multipliers. Then, the local Lagrange multiplier basis function μ_i at a node x_i of T is chosen to be a polynomial

of minimal degree such that $\mu_i(x_j) = \delta_{ij}$ for all x_j, $j = 1, \cdots, n$. Here, δ_{ij} is the Kronecker delta. These Lagrange multiplier basis functions are continuous. Since, in general, $M_h(\gamma_k) \subset \left(H^{1/2}(\gamma_k)\right)'$, we can work with discontinuous Lagrange multipliers. Working with a continuous Lagrange multiplier space which locally contains the linear functions has the advantage that assumption [P1] is satisfied. Here too, assumption [P0] is trivially satisfied by construction. To verify assumption [P2], we take $\varphi := \sum_{k=1}^{n_k} a_k \varphi_k$ in $W_{0,h}(\gamma_k)$ and define $\mu := \sum_{k=1}^{n_k} a_k \mu_k$. Then

$$(\varphi, \mu)_{0,\gamma_k} = \sum_{i,j=1}^{n_k} a_i a_j (\varphi_i, \mu_j)_{0,\gamma_k} = \sum_{i,j=1}^{n_k} a_i a_j \int_{\gamma_k} \varphi_i \, \mu_j \, d\sigma.$$

The local mass matrix $M_{\hat{T}}$ for an element having all the vertices in γ_k is given by

$$M_{\hat{T}} = \begin{bmatrix} \frac{1}{30} & \frac{1}{90} & \frac{1}{60} & \frac{1}{90} & -\frac{1}{30} & -\frac{2}{45} & -\frac{2}{45} & -\frac{1}{30} \\ \frac{1}{90} & \frac{1}{30} & \frac{1}{90} & \frac{1}{60} & -\frac{1}{30} & -\frac{1}{30} & -\frac{2}{45} & -\frac{2}{45} \\ \frac{1}{60} & \frac{1}{90} & \frac{1}{30} & \frac{1}{90} & -\frac{2}{45} & -\frac{1}{30} & -\frac{1}{30} & -\frac{2}{45} \\ \frac{1}{90} & \frac{1}{60} & \frac{1}{90} & \frac{1}{30} & -\frac{2}{45} & -\frac{2}{45} & -\frac{1}{30} & -\frac{1}{30} \\ -\frac{1}{30} & -\frac{1}{30} & -\frac{2}{45} & -\frac{2}{45} & \frac{8}{45} & \frac{1}{9} & \frac{4}{45} & \frac{1}{9} \\ -\frac{2}{45} & -\frac{1}{30} & -\frac{1}{30} & -\frac{2}{45} & \frac{1}{9} & \frac{8}{45} & \frac{1}{9} & \frac{4}{45} \\ -\frac{2}{45} & -\frac{2}{45} & -\frac{1}{30} & -\frac{1}{30} & \frac{4}{45} & \frac{1}{9} & \frac{8}{45} & \frac{1}{9} \\ -\frac{1}{30} & -\frac{2}{45} & -\frac{2}{45} & -\frac{1}{30} & \frac{1}{9} & \frac{4}{45} & \frac{1}{9} & \frac{8}{45} \end{bmatrix}.$$

Similarly, computing the local mass matrices for the different boundary cases, we find that all the eigenvalues of the local mass matrices are greater than $\frac{1}{100}$ and smaller than $\frac{6}{11}$. Then $(\varphi, \mu)_{0,\gamma_k}$, $\|\varphi\|^2_{0,\gamma_k}$ and $\|\mu\|^2_{0,\gamma_k}$ are equivalent to $\sum_{i=1}^{n_k} h^2_{s(k)} a_i^2$, which guarantees assumption [P2]. The coupling of the local mass matrices yield a global mass matrix which is sparse but has a band structure of band-width $O(1/h)$. Thus, the inverse of the global mass matrix M_s on the slave side is dense. As a consequence, we obtain a stiffness matrix associated with the variational problem (3), which is not sparse. Then we cannot apply static condensation, and the multigrid method discussed in [WK01] cannot be used.

To overcome this difficulty, we introduce a new approach for the serendipity elements. The idea is to use a Lagrange multiplier space which yields a sparse inverse of the global mass matrix M_s on the slave side. In this case, we use the tensor product Lagrange multiplier space introduced in Subsection 3.1. To satisfy the condition $\dim W_{0,h}(\gamma_k) = \dim M_h(\gamma_k)$, each non-empty face $f \subseteq \partial T \cap \Gamma$ of the element T of the slave side is enriched with a bubble function. The bubble function $b \in H^1(T)$ corresponding to the face f of T has the property that $b_{|\partial T \setminus f} = 0$ and $\int_f b \, d\sigma \neq 0$. We define $\mathcal{K}_s := \{T \in \mathcal{T}_{s(k);h_{s(k)}}, 1 \leq k \leq N \,|\, \partial T \cap \Gamma \text{ contains at least a face of } T\}$, the set of elements on the slave side each of which has at least one face f on Γ. Now, the space of bubble functions B_h is formed by N_s bubbles, where N_s is the number of elements in $\cup_{k=1}^{N} \mathcal{S}_{k;h_k}$, and each of them is corresponding to a face f of an element $T \in \mathcal{K}_s$, where $f \subseteq \partial T \cap \Gamma$. This leads to one additional degree of freedom for each non-empty face $f \subseteq \partial T \cap \Gamma$ of $T \in \mathcal{K}_s$. There are many possibilities to define such a bubble function. Here, the triquadratic nodal finite element function associated with the center of gravity of the face is used as a bubble function corresponding to this face. Although we need only the restriction of bubble functions to the associated face to satisfy assumption [P0], each bubble function is supported on the whole element. Now, the

modified unconstrained product space X_h^t can be written as $X_h^t = X_h^s \oplus B_h$, where X_h^s is the unconstrained product space associated with the serendipity elements. In the sequel, the space X_h^t will be called augmented serendipity space and the corresponding elements augmented serendipity elements. This leads to a mass matrix M_s on the slave side having a special structure. Suppose $\hat{\varphi}_i$ and $\hat{\lambda}_i$, $(1 \leq i \leq 9)$ be the local basis functions of the standard triquadratic finite elements and their dual Lagrange multipliers, respectively. Here, the first four basis functions correspond to the vertices, the second four ones correspond to the midpoints of the edges, and the last one corresponds to the center of gravity of the reference element $\hat{T}$. Then, the local basis functions of the serendipity elements can be written as $\hat{\varphi}_i^s = \hat{\varphi}_i + \alpha_i \hat{\varphi}_9$, $(1 \leq i \leq 8)$, where $\alpha_i = -\frac{1}{4}$ for $(1 \leq i \leq 4)$ and $\alpha_i = \frac{1}{2}$ for $(5 \leq i \leq 8)$. Using the biorthogonality of $\hat{\varphi}_i$ and $\hat{\lambda}_i$, we have

$$\int_{\hat{T}} \hat{\varphi}_i^s \, \hat{\lambda}_j \, d\sigma = \int_{\hat{T}} (\hat{\varphi}_i + \alpha_i \hat{\varphi}_9) \, \hat{\lambda}_j \, d\sigma = \delta_{ij} \int_{\hat{T}} \hat{\varphi}_i \, d\sigma + \alpha_i \delta_{9j} \int_{\hat{T}} \hat{\varphi}_9 \, d\sigma.$$

In fact, the mass matrix on the reference element $\hat{T}$ is

$$M_{\hat{T}} = \begin{bmatrix} \frac{1}{36} & 0 & 0 & 0 & 0 & 0 & 0 & 0 & 0 \\ 0 & \frac{1}{36} & 0 & 0 & 0 & 0 & 0 & 0 & 0 \\ 0 & 0 & \frac{1}{36} & 0 & 0 & 0 & 0 & 0 & 0 \\ 0 & 0 & 0 & \frac{1}{36} & 0 & 0 & 0 & 0 & 0 \\ 0 & 0 & 0 & 0 & \frac{1}{9} & 0 & 0 & 0 & 0 \\ 0 & 0 & 0 & 0 & 0 & \frac{1}{9} & 0 & 0 & 0 \\ 0 & 0 & 0 & 0 & 0 & 0 & \frac{1}{9} & 0 & 0 \\ 0 & 0 & 0 & 0 & 0 & 0 & 0 & \frac{1}{9} & 0 \\ -\frac{1}{9} & -\frac{1}{9} & -\frac{1}{9} & -\frac{1}{9} & \frac{2}{9} & \frac{2}{9} & \frac{2}{9} & \frac{2}{9} & \frac{4}{9} \end{bmatrix}. \tag{13}$$

To show the consequence of our new Lagrange multiplier space, we consider the global mass matrix M_s on the slave side in more detail. In the following, we use the same notation for the vector representation of the solution and the solution as an element in X_h^t and M_h. The matrix A is the stiffness matrix associated with the bilinear form $a(\cdot,\cdot)$ on $X_h^t \times X_h^t$, and the matrices B and B^T are associated with the bilinear form $b(\cdot,\cdot)$ on $X_h^t \times M_h$. Then, the algebraic formulation of the saddle point problem (4) is given by

$$\begin{bmatrix} A & B^T \\ B & 0 \end{bmatrix} \begin{bmatrix} u_h \\ \lambda_h \end{bmatrix} = \begin{bmatrix} f_h \\ 0 \end{bmatrix}. \tag{14}$$

We recall the grouping of the degrees of freedom of X_h^t introduced in Section 1. After augmenting the serendipity space with the space of bubble functions B_h, we further decompose the degrees of freedom associated with the interior nodes of $\gamma_k, 1 \leq k \leq N$, on the slave side into two groups (u_s, u_b). Here, the block vector u_s contains nodal values of u at the interior nodes of γ_k, $1 \leq k \leq N$, corresponding to the vertices and edges on the slave side, and u_b stands for all nodal values corresponding to the bubble functions on the slave side. With this decomposition, we can write $u_h^T = (u_i^T, u_m^T, u_s^T, u_b^T)$. The block vector λ_h containing the nodal values of the Lagrange multiplier is similarly decomposed with $\lambda_h^T = (\lambda_s^T, \lambda_b^T)$. In terms of this decomposition, we can rewrite the algebraic form of the

saddle point problem (14) as

$$\begin{bmatrix} A_{ii} & A_{im} & A_{is} & A_{ib} & 0 & 0 \\ A_{mi} & A_{mm} & A_{ms} & A_{mb} & M_m^T & M_{bm}^T \\ A_{si} & A_{sm} & A_{ss} & A_{sb} & D_s & M_{bs}^T \\ A_{bi} & A_{bm} & A_{bs} & A_{bb} & 0 & D_b \\ 0 & M_m & D_s & 0 & 0 & 0 \\ 0 & M_{bm} & M_{bs} & D_b & 0 & 0 \end{bmatrix} \begin{bmatrix} u_i \\ u_m \\ u_s \\ u_b \\ \lambda_s \\ \lambda_b \end{bmatrix} = \begin{bmatrix} f_i \\ f_m \\ f_s \\ f_b \\ 0 \\ 0 \end{bmatrix}. \tag{15}$$

Recalling the algebraic structure (5) of the bilinear form $b(\cdot,\cdot)$ restricted to $X_h^t \times M_h$, we have

$$B = \begin{bmatrix} M_m & D_s & 0 \\ M_{bm} & M_{bs} & D_b \end{bmatrix},$$

where D_b and D_s are diagonal matrices, and M_{bs}, M_m and M_{bm} are rectangular matrices. The matrix D_b is diagonal due to the fact that the bubble functions are supported only in one element, and the diagonal form of D_s follows from the structure of the local mass matrix, see (13). Hence, the global mass matrix M_s on the slave side can be written as

$$M_s = \begin{bmatrix} D_s & 0 \\ M_{bs} & D_b \end{bmatrix}.$$

The great benefit of this Lagrange multiplier space is that the inverse of the mass matrix M_s can be computed very easily, and the inverse is sparse. In fact, the inverse of the mass matrix M_s is

$$M_s^{-1} = \begin{bmatrix} {D_s}^{-1} & 0 \\ -D_b^{-1} M_{bs} D_s^{-1} & {D_b}^{-1} \end{bmatrix}.$$

Thus, the solution at the slave side depends locally on the solution at the master side. Here, we have to invert only two diagonal matrices and scale M_{bs} to compute the inverse of the mass matrix M_s. The stiffness matrix associated with the variational problem (3) is sparse, and efficient iterative solver like multigrid can easily be adapted to the nonconforming situation. Additionally, the condition number of the mass matrix is better compared to the standard Lagrange multiplier space. Furthermore, the degree of freedom corresponding to the bubble functions can locally be eliminated by static condensation. Since the matrix D_b is diagonal, the sixth and the fourth line of the system (15) give

$$\begin{aligned} u_b &= -D_b^{-1}(M_{bm}u_m + M_{bs}u_s), \quad \text{and} \\ \lambda_b &= D_b^{-1}\left[f_b - A_{bi}u_i - (A_{bm} - A_{bb}D_b^{-1}M_{bm})u_m - (A_{bs} - A_{bb}D_b^{-1}M_{bs})u_s\right]. \end{aligned}$$

Now, we eliminate u_b and λ_b from the system (15) and obtain a new system

$$\hat{A}\hat{u}_h = \hat{F}_h,$$

where $\hat{u}_h^T = (u_i^T, u_m^T, u_s^T, \lambda_s^T)$. Defining $M_1 := D_b^{-1}M_{bm}$ and $M_2 := D_b^{-1}M_{bs}$ we have

$$\hat{A} = \begin{bmatrix} A_{ii} & A_{im} - A_{ib}M_1 & A_{is} - A_{ib}M_2 & 0 \\ A_{mi} - M_1^T A_{bi} & A_{mm} - A_{mb}M_1 - M_1^T(A_{bm} - A_{bb}M_1) & A_{ms} - A_{mb}M_2 - M_1^T(A_{bs} - A_{bb}M_2) & M_m^T \\ A_{si} - M_2^T A_{bi} & A_{sm} - A_{sb}M_1 - M_2^T(A_{bm} - A_{bb}M_1) & A_{ss} - A_{sb}M_2 - M_2^T(A_{bs} - A_{bb}M_2) & D_s \\ 0 & M_m & D_s & 0 \end{bmatrix},$$

and the right hand side can be written as

$$\hat{F}_h = \begin{bmatrix} f_i \\ f_m - M_1^T f_b \\ f_s - M_2^T f_b \\ 0 \end{bmatrix}.$$

We observe that the matrix $\hat{A}$ is symmetric, if A is symmetric and it has exactly the same structure as the saddle point matrix arising from mortar finite element method with a dual Lagrange multiplier space, see [Woh01]. Because of this structure of the algebraic system, we can apply the multigrid method proposed in [WK01].

Remark 7. *There is also a possibility to use wavelets to get a mass matrix of special structure so that the inversion can be cheaper, and the inverse is sparse. In [Ste00], locally supported and piecewise polynomial wavelets are studied on non-uniform meshes which give a lower triangular mass matrix with higher order finite elements in triangular meshes.*

4 Numerical results

Here, we present some numerical examples in 3D for linear and quadratic mortar finite elements. We consider three different cases for quadratic mortar finite elements. The first one is the standard triquadratic finite element space with the dual Lagrange multiplier space introduced in Subsection 3.1. The second one is the serendipity space with a standard Lagrange multiplier space given in Subsection 3.2. Finally, the third one is the augmented serendipity space associated with the tensor product Lagrange multiplier space. Our numerical results show the same asymptotic behaviour as predicted by the theory. The implementation is based on the finite element toolbox ug, [BBJ$^+$97]. We do not discuss and analyze an iterative solver for the arising linear systems. Working with dual Lagrange multiplier spaces has the advantage that the flux can locally be eliminated, and static condensation yields a positive definite system on the unconstrained product space. In [WK01, Woh01], the modification of the system has been carried out and a local modification of the transfer operators of lower complexity has been proposed. The introduced multigrid has a level-independent convergence rate and is of optimal complexity. Unfortunately, in the case of a standard Lagrange multiplier space no local elimination of the flux can be carried out. Following the approach in [WK01], the sparsity of the modified system and the efficiency of the multigrid solver is lost. In that case, we apply a multigrid method for saddle point problems. This technique has been considered for mortar elements in [WW98] and further analyzed in [BDW99, WW02]. It turns out that we do not have to work in a positive definite subspace, and the smoother can be realized in an inner and outer iteration scheme. As in the other approach, level-independent multigrid convergence rates can be established. However, the numerical solution process is slower if we have to work with the saddle point approach. We point out that the more efficient multigrid method for the modified positive definite system can only be applied when the inverse of M_s is sparse, whereas the saddle point multigrid method is more general. Although we do not have a dual Lagrange multiplier space for the serendipity elements, the tensor product Lagrange multiplier space in combination with the introduction of bubble functions on the slave side of the interface yield an optimal discretization scheme. We present some numerical results in 3D illustrating the performance of the different Lagrange multiplier spaces. In particular,

we compare the discretization errors in the L^2- and H^1- norm for the solution for linear and quadratic mortar finite elements. The discretization errors in the flux across the interface are compared in a mesh-dependent Lagrange multiplier norm, which is defined by

$$\|\mu - \mu_h\|_h^2 := \sum_{m=1}^{N} \sum_{T \in \mathcal{S}_{m;h_m}} h_T \|\mu - \mu_h\|_{0,T}^2 \ ,$$

where h_T is the diameter of the element T. For all our examples, we have used uniform refinement. In each refinement step, one element is refined into eight subelements. We denote by X_h^l and X_h^f the unconstrained finite element spaces associated with the standard finite element spaces for the trilinear and the triquadratic case, respectively. Similarly, X_h^s and X_h^t are the unconstrained finite element spaces associated with the serendipity elements and the augmented serendipity elements as defined in the previous section, respectively. The corresponding solutions are denoted by u_h^l, u_h^f, u_h^s and u_h^t, respectively.

Remark 8. *We note that the concept of dual Lagrange multiplier spaces can be generalized to distorted hexahedral meshes. In that case, the mapping between the actual element and the reference element has a non-constant Jacobian. As a consequence, we have to compute for each face on the interface a biorthogonal basis with respect to local nodal one. This can be easily done by solving a local mass matrix system. By construction, the sum of the local dual Lagrange multiplier basis functions is one. Defining the global Lagrange multiplier basis functions by gluing the local ones together, we find that the constants are included in the Lagrange multiplier space. As a consequence, it is easy to verify that the discretization error is of order h for the lowest order conforming finite elements.*

Our first example is given by $-\Delta u = f$ on $\Omega := (0,1)^2 \times (0,2)$, where Ω is decomposed into two subdomains $\Omega_1 := (0,1)^3$ and $\Omega_2 := (0,1)^2 \times (1,2)$. The right hand side f and the boundary conditions are chosen such that the exact solution is given by $u(x,y,z) = 2\exp(-x^2 - y^2 - z^2)\sin(12\,yx)\,(x+y+z)\,(x-y-z)$. In Figure 4, the decomposition of the domain, the initial triangulation and the isolines of the solution at the interface $z = 1$ are shown. We have used a nonconforming initial triangulation, where the

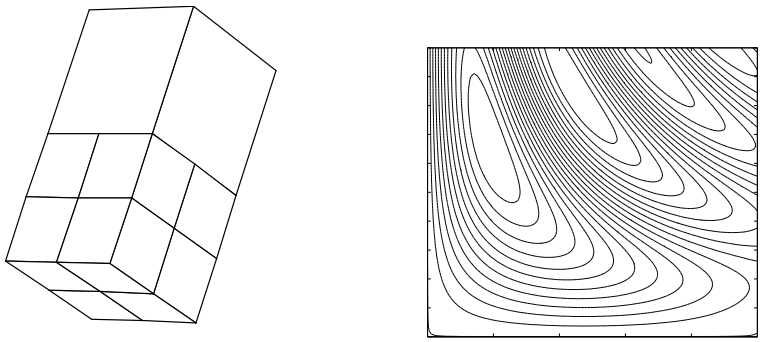

Figure 4: Decomposition of the domain and initial triangulation (left), isolines of the solution at the interface (right), Example 1

lower cube is refined once, and the upper cube is left as it is. The errors in the L^2-, H^1- and the weighted Lagrange multiplier norms are given in Tables 1–3. The tables show that we get the predicted asymptotic convergence rates. For the quadratic case, the errors in the L^2-

and H^1-norm are of order h^3 and h^2, whereas they are of order h^2 and h for the linear case. The errors in the weighted Lagrange multiplier norm for the quadratic and linear cases are of order $h^{5/2}$ and $h^{3/2}$, respectively. Theoretically, the errors in the weighted Lagrange multiplier norm for quadratic and linear case are expected to be of order h^2 and h, respectively. The better convergence rates are due to the fact that the error in the H^1-norm is equally distributed and the Lagrange multiplier space has an $O(h^{5/2})$ and $O(h^{3/2})$ approximation property in the considered norm. For the three different second order approaches, the quantitative results are asymptotically almost the same in the L^2- and H^1-norm. Only in the weighted Lagrange multiplier norm, the full triquadratic yields better results.

Table 1: Discretization errors in the L^2-norm, (Example 1)

level	# elem.	$\|u-u_h^l\|_0$	$\|u-u_h^f\|_0$	$\|u-u_h^s\|_0$	$\|u-u_h^t\|_0$
0	9	1.004794e+00	8.867203e-01	9.145121e-01	9.125653e-01
1	72	9.091292e-01	3.187528e-01	4.650386e-01	4.574443e-01
2	576	4.363422e-01	3.705310e-02	4.563530e-02	4.558460e-02
3	4608	1.033778e-01	7.450696e-03	7.649595e-03	7.611510e-03
4	36864	2.640337e-02	9.606873e-04	9.654041e-04	9.639183e-04

Table 2: Discretization errors in the H^1-norm, (Example 1)

level	# elem.	$\|u-u_h^l\|_1$	$\|u-u_h^f\|_1$	$\|u-u_h^s\|_1$	$\|u-u_h^t\|_1$
0	9	1.000886e+00	9.356647e-01	9.705044e-01	9.671180e-01
1	72	9.446222e-01	6.608442e-01	7.237820e-01	7.076152e-01
2	576	6.449633e-01	1.353106e-01	1.490407e-01	1.485072e-01
3	4608	3.005969e-01	4.988503e-02	5.140438e-02	5.108725e-02
4	36864	1.508831e-01	1.261993e-02	1.269328e-02	1.267161e-02

Table 3: Discretization errors in the weighted Lagrange multiplier norm, (Example 1)

level	# elem.	$\|\lambda-\lambda_h^l\|_h$	$\|\lambda-\lambda_h^f\|_h$	$\|\lambda-\lambda_h^s\|_h$	$\|\lambda-\lambda_h^t\|_h$
0	9	4.685044e-01	5.949429e+00	6.980608e+00	8.650037e+00
1	72	3.072290e+00	4.254093e+00	4.300310e+00	5.528655e+00
2	576	1.824458e+00	4.052985e-01	6.517151e-01	7.399415e-01
3	4608	6.300125e-01	1.071732e-01	1.493473e-01	1.466488e-01
4	36864	2.246235e-01	1.669782e-02	2.047104e-02	2.410364e-02

In Example 2, we choose a L-shaped domain. The domain $\Omega := ((0,1)^2 \times (0,2)) \cup ([1,2) \times (0,1)^2)$ is decomposed into three cubes, $\Omega_1 := (0,1)^3, \Omega_2 := (0,1)^2 \times (1,2)$ and $\Omega_3 := (1,2) \times (0,1)^2$. We have shown the decomposition of the domain and the initial triangulation in the left picture of Figure 5, and the isolines of the solution at the interface $z = 1$ are shown in the right. As before, we solve a Poisson problem

$$-\Delta u = f$$

with the right hand side function f and the Dirichlet boundary conditions determined by the exact solution $u(x,y,z) = \left((x-1)^2 + (z-1)^2\right)^{5/6} \cos\left(6\,y^2 + x^2 + 6\right)$.

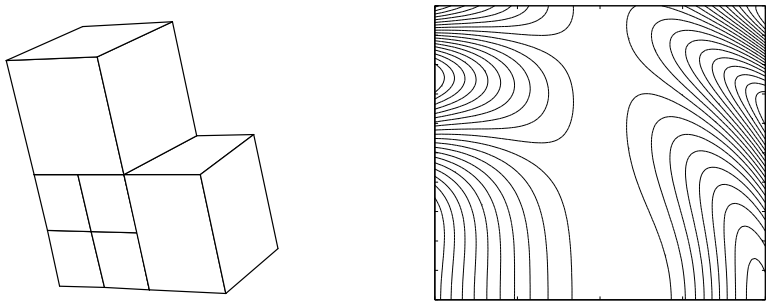

Figure 5: Decomposition of the domain and initial triangulation (left), isolines of the solution at the interface $z = 1$ (right), Example 2

We have tabulated the errors in different norms in Tables 4–6. Here, the solution is not H^3-regular. Therefore, we cannot expect the same order of convergence as in the previous example. Since the solution $u \in H^{8/3-\epsilon}(\Omega)$ for $\epsilon > 0$, we expect the same order of convergence as in the previous example in the linear case. In the quadratic case, theoretically the orders of $h^{8/3}$ and of $h^{5/3}$ are expected in the L^2- and H^1-norm, respectively. In all three cases of quadratic finite elements, we observe the asymptotic rates in the L^2- and H^1-norm, which are better than predicted by the theory. The quantitative results are also almost the same in these norms. Here too, we observe the better convergence rates for the errors in the weighted Lagrange multiplier norm.

Table 4: Discretization errors in the L^2-norm, (Example 2)

level	# elem.	$\|u-u_h^l\|_0$	$\|u-u_h^f\|_0$	$\|u-u_h^s\|_0$	$\|u-u_h^t\|_0$
0	10	1.327466e+00	7.318159e-01	8.066003e-01	7.957931e-01
1	80	8.047675e-01	1.748627e-01	2.039559e-01	2.008262e-01
2	640	2.057468e-01	4.863715e-02	4.936495e-02	4.910636e-02
3	5120	6.722455e-02	6.422065e-03	6.451969e-03	6.443622e-03
4	40960	1.766195e-02	8.056078e-04	8.064556e-04	8.066527e-04

In Examples 1 and 2, there is not any significant difference in the accuracy between the different quadratic mortar solutions either in the L^2-norm or in the H^1-norm. However, there is some quantitative difference in the errors in the weighted Lagrange multiplier norm between different quadratic mortar solutions. In this norm, the standard triquadratic finite elements with the tensor product Lagrange multiplier space gives the best result, whereas the difference between the augmented serendipity elements with the tensor product Lagrange multiplier space and the serendipity elements with the standard Lagrange multiplier space is quite negligible in Example 2. In Example 1, the serendipity elements with the standard Lagrange multiplier space yields better result than the augmented serendipity elements with the tensor product Lagrange multiplier space. However, the difference is not

Table 5: Discretization errors in the H^1-norm, (Example 2)

level	# elem.	$\|u-u_h^l\|_1$	$\|u-u_h^f\|_1$	$\|u-u_h^s\|_1$	$\|u-u_h^t\|_1$
0	10	1.021784e+00	8.085453e-01	8.194130e-01	8.049068e-01
1	80	8.094756e-01	3.934127e-01	4.259780e-01	4.159907e-01
2	640	4.221967e-01	1.803404e-01	1.831986e-01	1.814987e-01
3	5120	2.479979e-01	4.695275e-02	4.711321e-02	4.701404e-02
4	40960	1.277419e-01	1.173059e-02	1.173325e-02	1.173569e-02

Table 6: Discretization errors in the weighted Lagrange multiplier norm, (Example 2)

level	# elem.	$\|\lambda-\lambda_h^l\|_h$	$\|\lambda-\lambda_h^f\|_h$	$\|\lambda-\lambda_h^s\|_h$	$\|\lambda-\lambda_h^t\|_h$
0	10	9.992731e-01	5.988951e+00	4.678395e+00	7.046350e+00
1	80	2.416457e+00	1.831235e+00	3.100680e+00	2.018278e+00
2	640	8.795363e-01	5.338894e-01	7.909840e-01	6.360541e-01
3	5120	4.481377e-01	7.548844e-02	9.720802e-02	1.002547e-01
4	40960	1.720963e-01	1.157310e-02	1.577079e-02	1.684356e-02

essential, and the asymptotic convergence orders are the same. We remark that for both of these examples the asymptotic phase starts from the third step. This is due to the fact that the initial triangulation is very coarse.

For the next two examples, we consider only the serendipity elements. In our third example, the domain $\Omega := (0,1)^2 \times (0,2.5)$ is decomposed into three subdomains $\Omega_1 := (0,1)^3$, $\Omega_2 := (0,1)^2 \times (1,2)$, and $\Omega_3 := (0,1)^2 \times (2,2.5)$. The right hand side f and the boundary conditions of $-\Delta u = f$ are chosen such that the exact solution is given by $u(x,y,z) = 5(z-1.4)((x-0.5)^2+4(y-0.3)^3) + z(z-1)\sin(4\pi xy)(2(x-y)^2+(y+x-1)^2)$. In Figure 6, we have shown the decomposition of the domain, the initial nonmatching triangulation and the isolines of the solution at the interface $z = 2$.

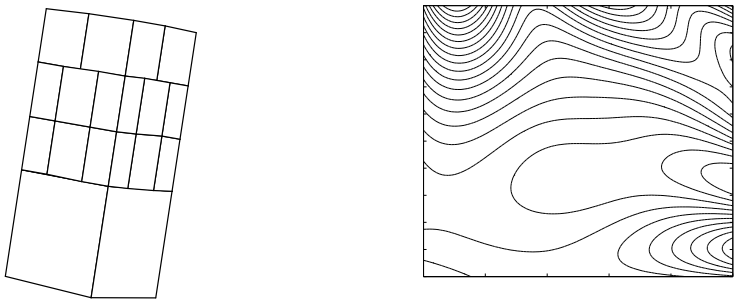

Figure 6: Decomposition of the domain and initial triangulation (left), isolines of the solution at the interface $z = 2$ (right), Example 3

Here, we have three subdomains and two interfaces. The middle cube is taken as the slave

side. We start with a nonconforming coarse initial triangulation having 23 elements. The errors along with their order of convergence at every step of refinement in different norms are given in Tables 7–9. As before, we get the correct asymptotic rates for both cases of the serendipity elements, and the errors in the L^2- and H^1-norm are almost the same for both approaches. In the weighted Lagrange multiplier norm the serendipity elements yield less errors than the augmented serendipity elements. However, the difference is quite negligible, and the asymptotic rate of convergence is optimal in both cases.

Table 7: Discretization errors in the L^2-norm, (Example 3)

level	# elem.	$\|u-u_h^l\|_0$		$\|u-u_h^s\|_0$		$\|u-u_h^t\|_0$	
0	23	8.911337e-01		1.745670e-01		1.760480e-01	0
1	184	2.582954e-01	1.79	2.997997e-02	2.54	3.010899e-02	2.55
2	1472	6.366337e-02	2.02	3.664595e-03	3.03	3.671731e-03	3.04
3	11776	1.607229e-02	1.99	4.466631e-04	3.04	4.462098e-04	3.04
4	94208	4.031862e-03	2.00	5.393667e-05	3.05	5.391429e-05	3.05

Table 8: Discretization errors in the H^1-norm, (Example 3)

level	# elem.	$\|u-u_h^l\|_1$		$\|u-u_h^s\|_1$		$\|u-u_h^t\|_1$	
0	23	8.170532e-01		5.517577e-01		5.290887e-01	0
1	184	5.643329e-01	0.53	1.478160e-01	1.90	1.482833e-01	1.84
2	1472	2.626420e-01	1.10	3.915936e-02	1.92	3.920488e-02	1.92
3	11776	1.293053e-01	1.02	9.352708e-03	2.07	9.332480e-03	2.07
4	94208	6.446694e-02	1.00	2.295583e-03	2.03	2.293897e-03	2.02

Table 9: Discretization errors in the weighted Lagrange multiplier norm, (Example 3)

level	# elem.	$\|\lambda-\lambda_h^l\|_h$		$\|\lambda-\lambda_h^s\|_h$		$\|\lambda-\lambda_h^t\|_h$	
0	23	7.433164e+00		2.762317e+01		2.758347e+01	0
1	184	5.657720e+00	0.39	2.006842e+00	3.78	3.320707e+00	3.05
2	1472	1.855735e+00	1.61	7.048806e-01	1.51	8.042462e-01	2.05
3	11776	4.868778e-01	1.93	1.001359e-01	2.82	1.151919e-01	2.80
4	94208	1.832775e-01	1.41	1.564914e-02	2.68	1.879805e-02	2.62

In our last example, we consider a domain $\Omega := (0,2)\times(0,1)\times(0,2)$, which is decomposed into four subdomains $\Omega_1 := (0,1)^3, \Omega_2 := (0,1)^2\times(1,2), \Omega_3 := (1,2)\times(0,1)^2$ and $\Omega_4 := (1,2)\times(0,1)\times(1,2)$. We have shown the decomposition of the domain and the initial triangulation in the left picture of Figure 7, the isolines of the solution on the plane $y=\frac{1}{2}$ in the middle, and the flux of the exact solution at the interface $x=1$ is shown in the right one. Here, Ω_2 and Ω_3 are taken to be the slave sides and the rest are the master sides. The problem for this example is given by a reaction-diffusion equation

$$-\mathrm{div}(a\nabla u)+u=f \quad \text{in} \quad \Omega,$$

where a is chosen to be 1 in Ω_1 and Ω_4, and $a = 10$ in Ω_2 and Ω_3. We have chosen the exact solution $u(x, y, z) = (x-1)\, y\, (z-1) \exp(-(x-1)^2 - y^2 - (z-1)^2) \cos(2\,x + 2\,y + 2\,z)\,/a$ and the right hand side f and the Dirichlet boundary conditions are determined from the exact solution. We remark that the exact solution u has a jump in the normal derivative

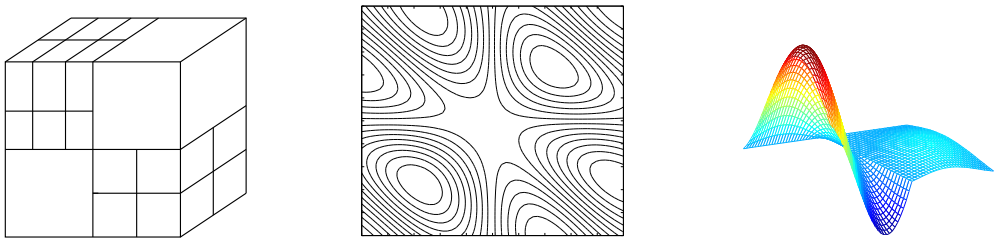

Figure 7: Decomposition of the domain and initial triangulation (left), isolines of the solution at the plane $y = \frac{1}{2}$ (middle) and flux of the exact solution at the interface $x = 1$ (right), Example 4

across the interface, whereas the flux is continuous. We have given the errors together with their order of convergence in every step of refinement in different norms in Tables 10–12. As in other examples, we get the same asymptotic rates for the L^2- and H^1-norm and better convergence rates in the weighted Lagrange multiplier norm. In contrast to other examples, we see that the asymptotic of errors in the weighted Lagrange multiplier norm for the quadratic case is even better than $O(h^3)$.

Table 10: Discretization errors in the L^2-norm, (Example 4)

level	# elem.	$\|u - u_h^l\|_0$		$\|u - u_h^s\|_0$		$\|u - u_h^t\|_0$	
0	22	4.636300e-01		1.237718e-01		1.233229e-01	
1	176	1.218875e-01	1.93	1.220035e-02	3.34	1.220072e-02	3.34
2	1408	3.082112e-02	1.98	1.164306e-03	3.39	1.164276e-03	3.39
3	11264	7.712933e-03	2.00	1.422899e-04	3.03	1.422876e-04	3.03
4	90112	1.928288e-03	2.00	1.773015e-05	3.00	1.773010e-05	3.00

Table 11: Discretization errors in the H^1-norm, (Example 4)

level	# elem.	$\|u - u_h^l\|_1$		$\|u - u_h^s\|_1$		$\|u - u_h^t\|_1$	
0	22	6.295650e-01		2.218643e-01		2.205473e-01	
1	176	3.009651e-01	1.06	4.609256e-02	2.27	4.607911e-02	2.26
2	1408	1.482825e-01	1.02	1.029429e-02	2.16	1.029336e-02	2.16
3	11264	7.379459e-02	1.01	2.523696e-03	2.03	2.523642e-03	2.03
4	90112	3.684966e-02	1.00	6.289388e-04	2.00	6.289362e-04	2.00

In both Examples 3 and 4, the discretization errors in the L^2- and H^1-norm are almost the same for different approaches. Concerning the discretization errors in the weighted Lagrange multiplier norm, although we see some quantitative difference in Examples 3 and

Table 12: Discretization errors in the weighted Lagrange multiplier norm, (Example 4)

level	# elem.	$\|\lambda - \lambda_h^l\|_h$		$\|\lambda - \lambda_h^s\|_h$		$\|\lambda - \lambda_h^t\|_h$	
0	22	8.588035e-02		6.184646e-02		8.310643e-02	
1	176	5.194191e-02	0.73	5.220039e-03	3.57	9.849865e-03	3.08
2	1408	2.538350e-02	1.03	4.361169e-04	3.58	7.810953e-04	3.66
3	11264	1.012701e-02	1.33	4.506948e-05	3.27	6.918887e-05	3.50
4	90112	3.755812e-03	1.43	5.074655e-06	3.15	6.546292e-06	3.40

4, we observe the better convergence rate for both approaches. In this norm, the serendipity elements with the standard Lagrange multiplier space gives better result in both examples. However, in Example 3, the order of convergence is almost the same for both approaches, whereas the augmented serendipity elements show the better order of convergence in Example 4. We already observe the better rate of convergence from the augmented serendipity elements from the second step of refinement.

In all our examples, we observe the optimal asymptotic convergence rates as predicted by the theory. Although we see the same qualitative behaviour, some quantitative differences can be observed. However, there is not any essential difference in the discretization errors between different quadratic mortar solutions. Because of the addition of bubble functions at the skeleton Γ, X_h^t has more degree of freedom than X_h^s. However, these bubble functions can locally be eliminated from the algebraic formulation of the saddle point problem leading to a system matrix, which is similar to the algebraic form of the saddle point problem arising from the mortar discretization with a dual Lagrange multiplier space. On the other hand, the growth rate of the number of bubble functions is only a factor of four in each refinement step, and restricted to the skeleton. This is negligible since we can work with the efficient multigrid solver in case of the augmented serendipity space with the tensor product Lagrange multiplier space. Although we can work with the efficient multigrid solver in case of standard triquadratic finite elements, the approach is not as optimal as the augmented serendipity approach due to the more degree of freedom and the growth rate of factor eight in each refinement step. It turns out that the most efficient approach is the one given by the augmented serendipity elements. The discretization errors are as good as in the other cases, and the numerical solution is cheaper.

References

[BBJ+97] P. Bastian, K. Birken, K. Johannsen, S. Lang, N. Neuß, H. Rentz–Reichert, and C. Wieners. UG – a flexible software toolbox for solving partial differential equations. *Computing and Visualization in Science*, 1:27–40, 1997.

[BD98] D. Braess and W. Dahmen. Stability estimates of the mortar finite element method for 3–dimensional problems. *East–West J. Numer. Math.*, 6:249–264, 1998.

[BDM90] C. Bernardi, N. Debit, and Y. Maday. Coupling finite element and spectral methods: First results. *Math. Comp.*, 54:21–39, 1990.

[BDW99] D. Braess, W. Dahmen, and C. Wieners. A multigrid algorithm for the mortar finite element method. *SIAM J. Numer. Anal.*, 37:48–69, 1999.

[Ben99] F. Ben Belgacem. The mortar finite element method with Lagrange multipliers. *Numer. Math.*, 84:173–197, 1999.

[BM97] F. Ben Belgacem and Y. Maday. The mortar element method for three dimensional finite elements. M^2AN, 31:289–302, 1997.

[BMP93] C. Bernardi, Y. Maday, and A.T. Patera. Domain decomposition by the mortar element method. In H. Kaper et al., editor, *Asymptotic and numerical methods for partial differential equations with critical parameters*, pages 269–286. Reidel, Dordrecht, 1993.

[BMP94] C. Bernardi, Y. Maday, and A.T. Patera. A new nonconforming approach to domain decomposition: the mortar element method. In H. Brezzi et al., editor, *Nonlinear partial differential equations and their applications*, pages 13–51. Paris, 1994.

[BS94] S.C. Brenner and L.R. Scott. *The Mathematical Theory of Finite Element Methods*. Springer–Verlag, New York, 1994.

[KLPV01] C. Kim, R.D. Lazarov, J.E. Pasciak, and P.S. Vassilevski. Multiplier spaces for the mortar finite element method in three dimensions. *SIAM J. Numer. Anal.*, 39:519–538, 2001.

[LW02] B.P. Lamichhane and B.I. Wohlmuth. Higher order dual Lagrange multiplier spaces for mortar finite element discretizations. *CALCOLO*, 39:219–237, 2002.

[SS00] P. Seshaiyer and M. Suri. Uniform hp convergence results for the mortar finite element method. *Math. of Comput.*, 69:521–546, 2000.

[Ste00] R. Stevenson. Locally supported, piecewise polynomial biorthogonal wavelets on non-uniform meshes. *Preprint 1157, Department of Mathematics, University of Utrecht*, 2000. to appear in Constr. Approx.

[WK01] B.I. Wohlmuth and R.H. Krause. Multigrid methods based on the unconstrained product space arising from mortar finite element discretizations. *SIAM J. Numer. Anal.*, 39:192–213, 2001.

[Woh01] B.I. Wohlmuth. *Discretization Methods and Iterative Solvers Based on Domain Decomposition*, volume 17 of *LNCS*. Springer Heidelberg, 2001.

[WW98] C. Wieners and B.I. Wohlmuth. The coupling of mixed and conforming finite element discretizations. In J. Mandel, C. Farhat, and X. Cai, editors, *Proceedings of the 10th International Conference on Domain Decomposition*, pages 546–553. AMS, Contemporary Mathematics series, 1998.

[WW02] C. Wieners and B. Wohlmuth. Duality estimates and multigrid analysis for saddle point problems arising from mortar discretizations. *Preprint SFB404/02-02, University of Stuttgart*, 2002. to appear in SISC.

Bishnu P. Lamichhane

Universität Stuttgart
Pfaffenwaldring 57
70569 Stuttgart
Germany

E-Mail: lamichhane@mathematik.uni-stuttgart.de

WWW: http://www.ians.uni-stuttgart.de/nmh/lamichhane/lamichhane.shtml

Barbara I. Wohlmuth

Universität Stuttgart
Pfaffenwaldring 57
70569 Stuttgart
Germany

E-Mail: wohlmuth@mathematik.uni-stuttgart.de

WWW: http://www.ians.uni-stuttgart.de/nmh/wohlmuth/wohlmuth.shtml

Erschienene Preprints ab Nummer 2003/001

Komplette Liste: `http://preprints.ians.uni-stuttgart.de`

2003/001 *Lamichhane, B. P., Wohlmuth, B. I.*: Mortar Finite Elements for Interface Problems.

2003/002 *Dryja, M., Gantner, A., Widlund, O. B., Wohlmuth, B. I.*: Multilevel Additive Schwarz Preconditioner For Nonconforming Mortar Finite Element Methods.

2003/003 *Klimke, A., Hanss, M.*: On the Reliability of the Influence Measure in the Transformation Method of Fuzzy Arithmetic.

2003/004 *Klimke, A.*: RANDEXPR: A Random Symbolic Expression Generator.

2003/005 *Klimke, A.*: How to Access Matlab from Java.

2003/006 *Merkle, T.*: Phase separation in solid mixtures under elastic loadings with application to solder materials.

2003/007 *Lamichhane, B. P., Wohlmuth, B. I.*: Second Order Lagrange Multiplier Spaces for Mortar Finite Elements in 3D.